Supporting Information

A Collagen-Immobilized Nanodevice for in Situ Ratiometric Imaging of Cancer Biomarkers in the Tumor Microenvironment

Fengyu Tian, Shurui Zhou, Shiyi Xie, Zhenhua Zhang, Ling Peng, Ling Jiang, Zeyuan Wang, Zhou Nie, and Yan Huang*

The State Key Laboratory of Chemo/Bio-Sensing and Chemometrics, College of Chemistry and Chemical Engineering, Hunan Provincial Key Laboratory of Biomacromolecular Chemical Biology, Hunan University, Changsha 410082, P. R. China

Corresponding author: yanhuang@hnu.edu.cn (Y. Huang);

Contents

Experimental Section

Materials and reagents

The recombinant human tumor necrosis factor-α (TNF-α), the human recombinant platelet-derived growth factor-BB (PDGF-BB), the human recombinant interferon-γ (IFN-γ), the human recombinant vascular endothelial growth factor (VEGF), and the human PDGF-BB mammalian expression plasmid (C-GFPSpark tag, HG10572-ACG) were purchased from Sino Biological Inc. (Beijing, China). Collagen III was purchased from Sigma-Aldrich (St. Louis, MO, USA). Bovine serum albumin (BSA), ATP, GTP, CTP, UTP, and the BCA Protein Assay Kit (C503021) were purchased from Sangon Biotech (Shanghai, China). Sodium chloride (NaCl), potassium chloride (KCl), magnesium chloride ($MgCl_2$•$6H_2O$), manganese dichloride ($MnCl_2$•$4H_2O$), 2-hydroxyethyl (Hepes), and the BCA Protein Assay Kit (C503021) were purchased from Sinopharm Chemical Reagent Co., Ltd. (Shanghai, China). Streptolysin O (SLO) and cell counting kit-8 (CCK-8) were purchased from Solarbio Science & Technology (Beijing, China). Lipo8000™ transfection reagent (Lipo8000) was purchased from Beyotime Biotechnology (Shanghai). The DMEM medium, fetal bovine serum (FBS), penicillin, and streptomycin were provided by Thermo Fisher (Waltham, USA). CELLSAVING was purchased from New Cell &Molecular Biotech (C40100). All chemical reagents were of analytical grade and used without further purification unless otherwise noted. Ultrapure water (18.25 MΩ·cm) was obtained from a Millipore Milli-Q ultrapure water system (Billerica, MA).

Sangon Biotech Co., Ltd. (Shanghai, China) synthesized and purified all the oligonucleotides. The oligonucleotides were dissolved in ultrapure water for a concentration of 20 μM and stored at -4°C for further use.

The components of the buffer solutions used in the experiment are listed as follows. 1× HUH buffer: 50 mM Hepes, 100 mM NaCl, 100 mM KCl, 1 mM Mg^{2+}, and 1 mM Mn^{2+}, pH 7.4; 1× PBS buffer: 136 mM NaCl, 8 mM Na_2HPO_4, 2 mM KH_2PO_4, and 2.6 mM KCl, pH 7.4; 1× PBS-HSA buffer: 136 mM NaCl, 8 mM Na_2HPO_4, 2 mM KH_2PO_4, 2.6 mM KCl, 1 mM Mg^{2+}, and 0.01% HSA, pH 7.4.

Construction and purification of CmD and mD

The amino acid sequences of CBD (A3 CBD of von Willebrand factor), DCV (HUH tag, duck

circovirus), and mCherry were referred to the previous studies and reversely translated according to the codon preference of *E. coli* [1-3]. The pET28a-*cbd* was constructed by Sangon Biotech. The genes of mCherry and DCV were amplified by PCR using Q5 high-fidelity DNA polymerase and customized specific primers. They were sequentially inserted into pET28a-*cbd* at XhoI/HindIII restriction sites, resulting in pET28a-*cbd-mcherry-dcv* (**Fig S1A**). Similarly, the construct pET28a-*mcherry-dcv* was obtained (**Fig S1B**). The CBD, mCherry, and DCV amino acid sequences are presented below. The dark gray sequence indicates the CBD domain, the red sequence indicates the GGGGS linker, the violet sequence shows the mCherry domain, and the blue line indicates the DCV domain.

cbd-mcherry-dcv (CmD)

MCSQPLDVILLLDGSSSFPASYFDEMKSFAKAFISKANIGPRLTQVSVLQYGSITTIDVPWN
VVPEKAHLLSLVDVMQREGGPSQIGDALGFAVRYLTSEMHGARPGASKAVVILVTDVSV
DSVDAAADAARSNRVTVFPIGIGDRYDAAQLRILAGPAGDSNVVKLQRIEDLPTMVTLGN
SFLHKLCSGFVRI*GGGSGGGSGS*LVVSKGEEDNMAIIKEFMRFKVHMEGSVNGHEFEIEGE
GEGRPYEGTQTAKLKVTKGGPLPFAWDILSPQFMYGSKAYVKHPADIPDYLKISFPEGFK
WERVMNFEDGGVVTVTQDSSLQDGEFIYKVKLRGTNFPSDGPVMQKKTMGWEASSER
MYPEDGALKGEIKQRLKLKDGGHYDAEVKTTYKAKKPVQIPGAYNVNIKLDITSHNEDY
TIVEQYERAEGRHSTGGMDELYK*GGSGGSGGSGGS*MAKSGNYSYKRWVFTINNPTFEDY
VHVLEFCTLDNCKFAIVGEEKGANGTPHLQGFLNLRSNARAAALEESLGGRAWISRARGS
DEDNEEYCAKESTYLRVGEPVSKGRSSDIAEATSAV

mcherry-dcv (mD)

LVVSKGEEDNMAIIKEFMRFKVHMEGSVNGHEFEIEGEGEGRPYEGTQTAKLKVTKGGP
LPFAWDILSPQFMYGSKAYVKHPADIPDYLKLSFPEGFKWERVMNFEDGGVVTVTQDSS
LQDGEFIYKVKLRGTNFPSDGPVMQKKTMGWEASSERMYPEDGALKGEIKQRLKLKDG
GHYDAEVKTTYKAKKPVQLPGAYNVNIKLDITSHNEDYTIVEQYERAEGRHSTGGMDEL
YK*GGSGGSGGSGGS*MAKSGNYSYKRWVFTINNPTFEDYVHVLEFCTLDNCKFAIVGEEK
GANGTPHLQGFLNLRSNARAAALEESLGGRAWLSRARGSDEDNEEYCAKESTYLRVGEP
VSKGRSSDLAEATSAV

The pET28a-*cbd-mcherry-dcv* and pET28a-*mcherry-dcv* constructs were transferred into *E. coli* BL21 DE3 (TIANGEN BIOTECH) by heat shock, respectively. Single clones were cultured in 5

mL liquid Luria-Bertani (LB) medium at 37°C overnight. Subsequently, 1% (v/v) of the culture was inoculated into 250 mL of fresh liquid LB and incubated at 37°C with shaking at 220 rpm until reaching the logarithmic growth phase. Protein expression was then induced by adding 0.4 mM isopropyl β-D-1-thiogalactopyranoside (IPTG) and incubating at 16°C for 16 h. Cells were harvested by centrifugation at 8000 rpm for 6 min at 4°C, transferred to the lysis buffer, and sonicated on ice for 30 min using an ultrasonic cell disruptor. Protein purification was performed using Ni-NTA agarose chromatography (ÄKTA, GE) after centrifugation at 10000 rpm for 20 min at 4°C. The purified protein kept in the buffer (20 mM Tris-HCl, 600 mM NaCl, 10% (v/v) glycerol, pH 7.4) was quantified using the BCA protein quantification kit and stored at -80°C. The molecular weight and fluorescence properties of the purified protein CmD and mD were then analyzed using SDS-PAGE and a fluorescence spectrophotometer SynergyTMMx multimode microplate reader (BioTek, USA), respectively.

Detection of CmD binding to collagen proteins and covalent linking to the ssDNA

The bifunctional properties of CmD binding to collagen and the ssDNA were assessed by SDS-PAGE and in vitro imaging, respectively.

CmD was mixed with a single-stranded DNA containing the DCV-specific recognition sequence ($ssDNA_{DCV}$) in a 1:1 ratio in the HUH buffer. The mixture was incubated at 37°C for 30 min to form a chimeric protein-nucleic acid conjugate (CmD-$ssDNA_{DCV}$). The product was analyzed by electrophoresis on a 12% stain-free polyacrylamide gel (AnyKD-PAGE Gel Rapid Preparation Kit). The binding capacity of CmD proteins to collagen was assessed using the collagen-coated 96-well plate. We prepared the covalent adducts (CmD-$ssDNA_{DCV}$-Cy5 and mD-$ssDNA_{DCV}$-Cy5) by conjugating Cy5-labeled $ssDNA_{DCV}$ ($ssDNA_{DCV}$-Cy5) to the fusion protein. Subsequently, the adducts were incubated in the collagen-coated wells and subjected to fluorescence imaging, respectively. Briefly, 100 μL of collagen type III (10 μg/mL) in the sodium acetate solution (50 mM) was added to a 96-well plate overnight at 4°C. The wells were then washed with PBS-T (1× PBS containing 0.05% Tween 20) and subsequently blocked with 2% BSA in PBS for 1 h at room temperature. After three washes with PBS-T, the wells were further incubated with CmD, CmD-$ssDNA_{DCV}$-Cy5, mD, or mD-$ssDNA_{DCV}$-Cy5 (1 μM) for 2 h at 37°C. After washing, the fluorescence signals of mCherry and Cy5 were measured in the 96-well plates using an inverted fluorescence microscope (Leica DMi8, Wetzlar, Germany) with an HC PL FLOOTAR 10×/0.32

numerical aperture dry objective. mCherry: excitation wavelength (E_x) 555 nm/emission wavelength (E_m) 610 nm; Cy5: E_x 635 nm/E_m 670 nm.

The time kinetics and stability of CmD binding to collagen were further evaluated using the same approach. All image analyses were performed with the basic functions of the Fiji software.

Construction of CPNN

The **CPNN** was obtained by covalently conjugating the DNA sensing module to the CmD. The preparation of the sensing module through sequential hybridization of the three strands with distinct functions.

S_{PDGF} was assembled by mixing a 5′-FAM-labelled PDGF-BB aptamer strand (Apt-FAM), a 3′-quencher-modified strand (cDNA-BHQ1) that complements the 5′ terminal sequence of Apt-FAM, and a DCV-specific recognition sequence-containing strand ($cDNA_{DCV}$) that complements the 3′ terminal sequence of Apt-FAM, in PBS buffer at a molar ratio of 1:3:1.2. The mixture was heated to 95°C for 10 min and slowly cooled to room temperature. Similarly, S_{ATP} was synthesized through the hybridization of ssDNA containing the aptamer and the DCV-specific recognition sequence (Apt_{DCV}) with 5′-Cy5-labeled cDNA (cDNA-Cy5) and 3′-quencher-modified cDNA (cDNA-Q_{ATP}) at a molar ratio of 1:1.5:2.

To obtain a chimeric protein-nucleic acid nanodevice (**CPNN**), S_{PDGF} or S_{ATP} was mixed with CmD or mD at a 1:1 ratio in the HUH buffer at 37°C for 30 min. The prepared CPNN was then stored at 4°C for further use.

CPNN-based target sensing in solution

The signal recognition of **CPNN** depends on its sensing module. Therefore, the function of S_{PDGF} was initially assessed in the buffer.

To assess the response of S_{PDGF} to PDGF-BB, S_{PDGF} (20 nM) was mixed with various concentrations of PDGF-BB in 1× PBS-HSA buffer, resulting in a total volume of 50 μL. The mixture was then incubated at 37°C for 60 min, and the fluorescence spectra of the solutions were recorded using a SynergyTM Mx multi-mode microplate reader with an excitation wavelength of 480 nm. Fluorescence kinetics were evaluated by measuring the fluorescence emission intensity at 520 nm using a SynergyTM Mx multi-mode microplate reader with 480 nm excitation every minute. To investigate the selectivity, S_{PDGF} was treated with TNF-α, IFN-γ, VEGF, and TGF-β, respectively, compared to PDGF-BB (100 nM).

To investigate the response of S_{ATP} to ATP, S_{ATP} was diluted to 200 nM in the HUH buffer. Subsequently, ATP at various concentrations was added to the solution and incubated at 37°C for 30 min. The fluorescence spectra of the resulting solutions were recorded using a SynergyTM Mx multi-mode microplate reader with an excitation wavelength of 650 nm. Additionally, the kinetics analysis and the specificity (ATP, GTP, CTP, and UTP) in response to ATP were also examined.

The sensing performance of **CPNN** was evaluated in the buffer using a similar detection procedure. The FAM/mCherry and Cy5/mCherry emission spectra were obtained by exciting the samples at 480 nm/580 nm and 650 nm/580 nm, respectively.

Calculation of fluorescence quantum yield of S_{PDGF} and $CPNN_{PDGF}$

The fluorescence quantum yield (Φ) was determined using Equation S1 [4]:

$$\Phi_{F(X)} = \Phi_{F(S)} (n_X / n_S)^2 A_S F_X / (A_X F_S) \qquad (S1)$$

In this equation, Φ represented the fluorescence quantum yield, A represented the absorbance at the excitation wavelength, F represented the area under the corrected emission curve, and n represented the refractive index of the solvent. Subscripts S and X denoted the standard and unknown, respectively. Notably, the absorbances of S_{PDGF}, $\mathbf{CPNN}_{PDGF}$, and the standard were maintained below 0.05.

Photostability of $CPNN_{PDGF}$

$\mathbf{CPNN}_{PDGF}$ (20 nM) was mixed with 20 nM PDGF-BB in 1× PBS-HSA buffer, resulting in a total volume of 50 μL. Following a 60-minute incubation at 37°C, we evaluated the photostability of $\mathbf{CPNN}_{PDGF}$ under extended excitation conditions. The photostability experiments were performed on the SynergyTM Mx multi-mode microplate reader with a 20 W xenon lamp for 180 min. The fluorescence emission intensity was measured every 10 min using the SynergyTM Mx multi-mode microplate reader.

CPNN-based target imaging in the collagen-coated plates

To obtain good imaging signals, FAM on the aptamer strand was replaced by Cy5 to construct **CPNN** and subsequent experiments. 96-microwell plates were coated with collagen type III (10 μg/mL) in the sodium acetate buffer for 12 h at 4°C, followed by blocking with 2% BSA in PBS with 0.05% Tween 20 (PBS-T) for 1 h at room temperature. Subsequently, the wells were washed with PBS-T and further incubated with **CPNN** (200 nM) for 2 h at 37°C. After three washes with PBS-T, the wells were incubated at 37°C in the buffer containing different concentrations of PDGF-

BB or ATP and subjected to imaging on a Leica DMi8 inverted microscope. Fluorescence channel E_x 555 nm/E_m 610 nm was used for mCherry, and E_x 635 nm/E_m 670 nm for Cy5.

All image analyses were performed with the essential functions of the software Image J. In the colocalization analysis of different fluorescent signals, we initially employed a Line tool to delineate the region of interest. Subsequently, the distribution of fluorescence signals within the selected area was obtained through the Plot Profile function. Finally, to generate fluorescence change curves at various positions within the chosen region, we exported data from different fluorescence channels and plotted them within a unified coordinate system. For a more intuitive comparison of the acquired fluorescence images, we employed Image J for a semi-quantitative analysis of the fluorescence signals within these images. We first used the Rectangle tool to draw the regions of interest and then selected the Measure function to obtain the average fluorescence intensity of the area.

Cell culture

Michigan cancer foundation-7 (MCF-7) cells were obtained from the cell bank of the central laboratory at Xiangya Hospital (Changsha, China). MCF-7 cells were cultured in DMEM (Gibco®, Life Technologies, Carlsbad, CA) supplemented with 10% (v/v) heat-inactivated FBS, 100 U penicillin, and streptomycin 0.1 mg/ml at 37°C in 5% CO_2.

Cytotoxicity assay

Cytotoxicity of CmD and **CPNN** was assessed using the CCK-8 assay. Cells (2×10^4 cells/mL, 100 μL) were seeded in 96-microwell plates and incubated at 37°C for 24 h. Subsequently, the cells were treated with varying concentrations of CmD and **CPNN** for 24 h, or the cells were treated with 1 μM CmD or **CPNN** for increasing incubation times (0, 2, 4, 6, 8, 12, 24 h), respectively. After washing with PBS, the cells were incubated with a fresh medium containing 10 % CCK-8 for an additional 2 h, and then the absorbance at 450 nm was measured using a multimode microplate reader. Cell viability (%) was calculated using the formula: Viability (%) = (mean Abs. of treated wells/mean Abs. of control wells) × 100. Each experiment was tested in 5 replicates.

Culture of the MCF-7 tumor spheroids

MCF-7 tumor spheroids were generated following the method reported previously with minor modifications [5]. Briefly, MCF-7 cells were trypsinized and resuspended in DMEM supplemented with FBS. Next, 200 μL of the solution containing cells at 2×10^4 cells/mL density was added to a 96-microwell plate pre-coated with 1.2% low-melting-temperature agarose (80 μL). The plate was

then incubated at 37°C for 2-3 days to facilitate the growth of cell spheres. The tumor spheroids were utilized in subsequent experiments once they reached the desired size.

For plasmid transfection on the tumor spheroids, MCF-7 cells (2×10^4 cells) were seeded in the agarose-coated 96-microwell plate and incubated at 37°C for 24 h before transfection. The plasmids were transiently transfected for 48 h using Lipo8000™ transfection reagent according to the manufacturer's protocol.

Immunofluorescence analysis of collagen in MCF-7 tumor spheroids

Collagen expression in the MCF-7 tumor spheroids was assessed through an indirect immunofluorescence assay. The MCF-7 tumor spheroids were briefly washed with cold PBS and then fixed overnight at 4°C in 4% paraformaldehyde. The MCF-7 tumor spheroids were then blocked with 2% BSA for 1 h to prevent non-specific binding of IgG following the PBS wash. Subsequently, the MCF-7 tumor spheroids were stained overnight at 4°C with a rabbit anti-collagen antibody (1:200; ab34710, Abcam), and then incubated with a goat anti-rabbit IgG (H+L) (Alexa Fluor 594) secondary antibody (1:1000; AWS0006a, Abiowell Biotechnology) for 1 h at room temperature. In control experiments, a goat anti-mouse IgG (H+L) (Alexa Fluor 594) secondary antibody (1:1000; AWS0004a, Abiowell Biotechnology) was utilized. The MCF-7 tumor spheroids were imaged using a Leica DMi8 inverted microscope after washing. The fluorescence signal of Alexa Fluor 594 was detected using the E_x 575 nm/E_m 610 nm channel. Images were processed using Image J software.

CPNN-based target imaging in the MCF-7 tumor spheroids

The MCF-7 tumor spheroids were treated with **CPNN** (200 nM) and incubated at 37°C for 30 min. After three washes with PBS-B buffer (PBS buffer containing 2% BSA), the MCF-7 tumor spheroids were incubated at 37°C for 60 min in a buffer with varying concentrations of PDGF-BB or ATP. Subsequently, the MCF-7 tumor spheroids were washed three times with PBS-B buffer and observed under an inverted microscope using an HC PL FLOOTAR 10×/0.32 numerical aperture dry objective.

PDGF-BB released from the genetically engineered (plasmid transfected) or wild-type MCF-7 tumor spheroids were quantified using **CPNN**. The MCTSs were treated with CRN-R (200 nM) and incubated at 37°C for 30 min. After three washes, the MCF-7 tumor spheroids were incubated at 37°C for 60 min in a buffer containing streptolysin O (SLO). Afterward, the MCF-7 tumor spheroids

were washed and resuspended in PBS for imaging.

For the analysis of ATP release, the MCF-7 tumor spheroids pre-anchored with **CPNN** were treated with different concentrations of SLO and then processed for imaging after washing and resuspension in PBS. Images were processed using Image J software.

Statistical analysis

Each experiment was replicated at least three times, and all replication attempts yielded consistent results. Statistical significance was assessed using a two-tailed Student's t-test unless stated otherwise. Curve fitting was conducted using Prism 8 (GraphPad), and P values were reported (not significant = $p > 0.05$, *$p \leq 0.05$, **$p \leq 0.01$, ***$p \leq 0.001$) and indicated on the figures. Error bars represent the standard deviation (S.D.)

Supplemental Tables

Table S1 Sequences of the oligonucleotides used for assessing the covalent coupling of DCV to single-stranded in fusion proteins.

Oligonucleotides	Sequences
$ssDNA_{DCV}$	AAG TAT TAC CAG AAA AAA
$ssDNA_{DCV}$-Cy5	AAG TAT TAC CAG AAA AAA-Cy5

Table S2 Sequences of the oligonucleotides for the construction of S_{PDGF}.

Oligonucleotides	Sequences
Apt_{35}-FAM	FAM-AAG GCT ACG GCA CGT AGA GCA TCA CCA TGA TCC TGT GTG GTC TAT GTC GTC GTT CG (35 nt)
Apt_{36}-FAM	FAM-A AAG GCT ACG GCA CGT AGA GCA TCA CCA TGA TCC TGT GTG GTC TAT GTC GTC GTT CG (36 nt)
Apt_{37}-FAM	FAM-AA AAG GCT ACG GCA CGT AGA GCA TCA CCA TGA TCC TGT GTG GTC TAT GTC GTC GTT CG (37 nt)
$mApt_{35}$-FAM	FAM-AAG GCT ACG GCA CGA TCT CGT AGT GGT CTG ACT GCT GTG GTC TAT GTC GTC GTT CG (35 nt)
$cDNA_{12}$-BHQ1	TGC CGT AGC CTT-BHQ1 (12 nt)
$cDNA_{13}$-BHQ1	TGC CGT AGC CTT T-BHQ1 (13 nt)
$cDNA_{14}$-BHQ1	TGC CGT AGC CTT TT-BHQ1 (14 nt)
$cDNA_{DCV}$	AAG TAT TAC CAG AAA CGA ACG ACG ACA TAG ACC ACA
$mApt_{35}$-Cy5	Cy5-AAG GCT ACG GCA CGA TCT CGT AGT GGT CTG ACT GCT GTG GTC TAT GTC GTC GTT CG
$cDNA_{12}$-BHQ3	TGC AGC CTT-BHQ3 (12 nt)

Table S3 Sequences of the oligonucleotides for the construction of S_{ATP}.

Oligonucleotides	Sequences
Apt_{DCV}	AAG TAT TAC CAG AAA CGC CTC GCA CCG TGG TCA CTG ACC TGG GGG AGT ATT GCG GAG GAA GGT
$mApt_{DCV}$	AAG TAT TAC CAG AAA CGC CTC GCA CCG TGG TCA CTG ACC TGG GGG AGT ATT GCA AAA ACA GGT
cDNA-$BHQ3_{ATP}$	CCA GGT CAG TG-BHQ3
cDNA-Cy5	Cy5-CCA CGG TGC GAG GCG

Table S4 Sequences of the oligonucleotides for the construction of S_{ATP}.

Oligonucleotides	Sequences
Apt_{DCV}	AAG TAT TAC CAG AAA CGC CTC GCA CCG TGG TCA CTG ACC TGG GGG AGT ATT GCG GAG GAA GGT
$mApt_{DCV}$	AAG TAT TAC CAG AAA CGC CTC GCA CCG TGG TCA CTG ACC TGG GGG AGT ATT GCA AAA ACA GGT
cDNA-$BHQ3_{ATP}$	CCA GGT CAG TG-BHQ3
cDNA-Cy5	Cy5-CCA CGG TGC GAG GCG

Table S5 Fluorescence quantum yield (Φ) and excitation maximum wavelength of fluorophores labeled on $\mathbf{S}_{PDGF}$ and $\mathbf{CPNN}_{PDGF}$ in the presence and absence of PDGF-BB.

Compound	Fluorophores	$\lambda_{ex}/\lambda_{em}$ (nm)	Φ	
			Without PDGF-BB	With PDGF-BB
[a] $\mathbf{S}_{PDGF}$	FAM/BHQ1	480/520	0.090	0.313
[b] $\mathbf{CPNN}_{PDGF}$	FAM/BHQ1	480/520	0.092	0.304
	mCherry	560/610	0.182	0.191
[c] $\mathbf{S}_{PDGF}$	Cy5/BHQ3	650/570	0.029	0.108
[d] $\mathbf{CPNN}_{PDGF}$	Cy5/BHQ3	650/570	0.031	0.115
	mCherry	560/610	0.174	0.185

[a] Φ of S_{PDGF} in the absence and presence of PDGF-BB was determined using FAM (Φ = 0.86) as a standard [6].

[b] Φ of $\mathbf{CPNN}_{PDGF}$ in the absence and presence of PDGF-BB was determined using FAM and mCherry (Φ = 0.22) as a standard, respectively [7].

[c] Φ of S_{PDGF} in the absence and presence of PDGF-BB was determined using Cy5 (Φ = 0.27) as a standard [8].

[d] Φ of $\mathbf{CPNN}_{PDGF}$ in the absence and presence of PDGF-BB was determined using Cy5 and mCherry as a standard, respectively.

Supplemental Figures

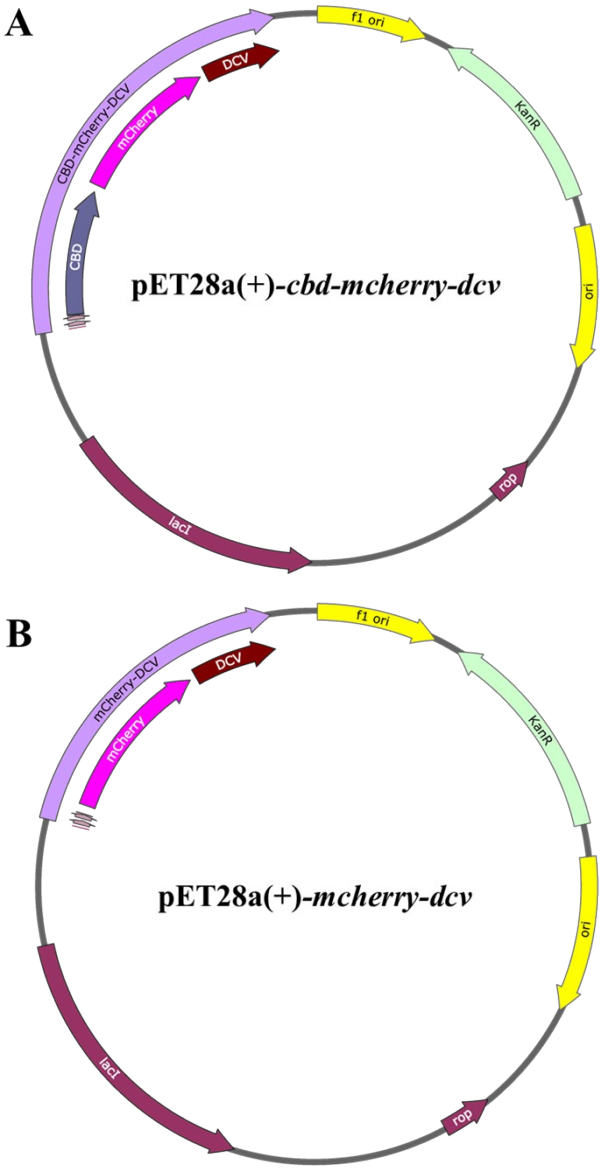

Figure S1. The maps of pET28a-*cbd-mcherry-dcv* and pET28a-*mcherry-dcv*. The plasmid pET28a (+) containing the T7 promoter (purple box) was used for expression of the fusion protein, including CBD (dark gray box), mCherry (violet box), and DCV (blue box).

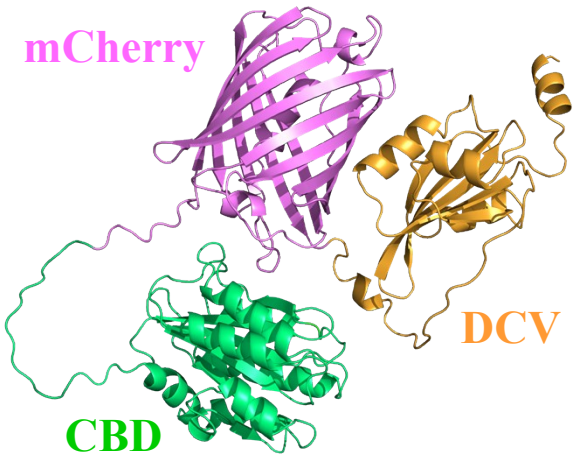

Figure S2. The structure of CmD as predicted by AlphaFold2.

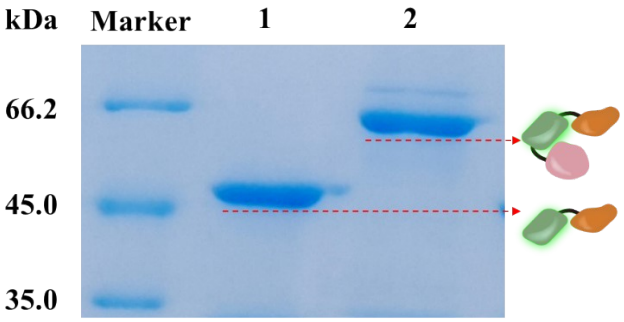

Figure S3. Verification of the biosynthesized CmD (65 kDa) and mD (46 kDa) through SDS-PAGE.

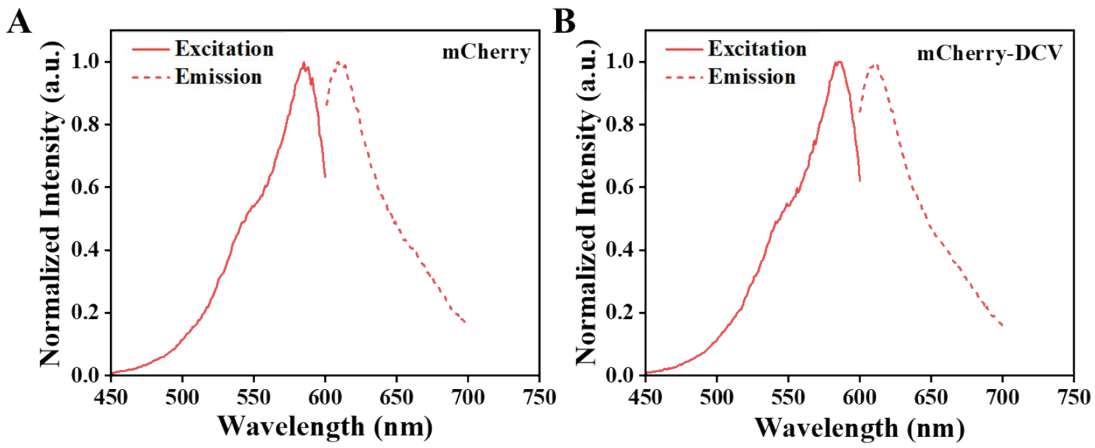

Figure S4. Fluorescence emission and excitation spectra of mCherry and mD.

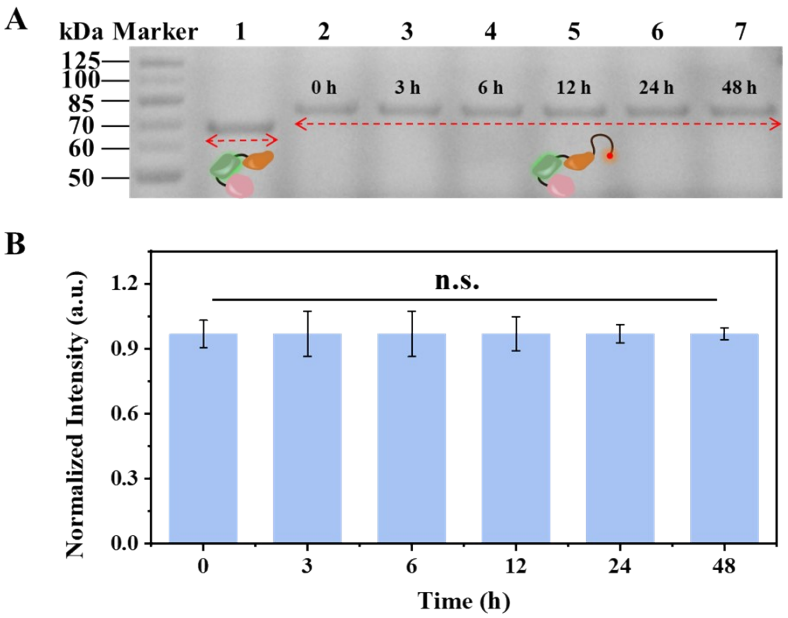

Figure S5. Stability analysis of CmD-ssDNA$_{DCV}$. (A) SDS-PAGE of the CmD-ssDNA$_{DCV}$ covalent adduct stored at 4°C for different times. (B) Semi-gel-band quantitation of CmD-ssDNA$_{DCV}$ in (A) using Image J. CmD, 1 μM; ssDNA$_{DCV}$ 1 μM.

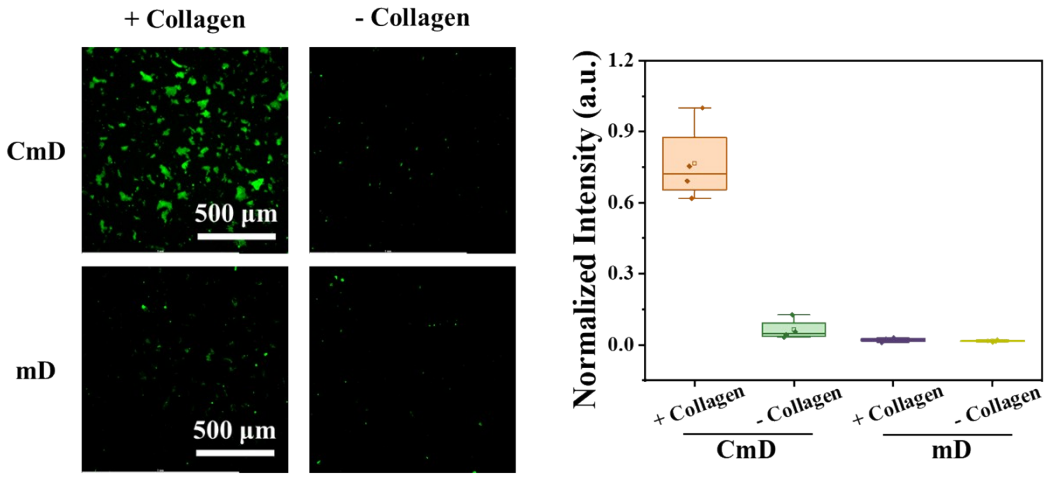

Figure S6. Assessing specific binding of CmD to collagen. Fluorescence images (left) and the corresponding fluorescence signals (right) of a microplate immobilized with CmD and mD in the presence and absence of type III collagen. Collagen III, 10 µg/mL; CmD, 1 µM; mD, 1 µM. mCherry: excitation wavelength (E_x) 555 nm/emission wavelength (E_m) 610 nm. Scale bar, 500 µm.

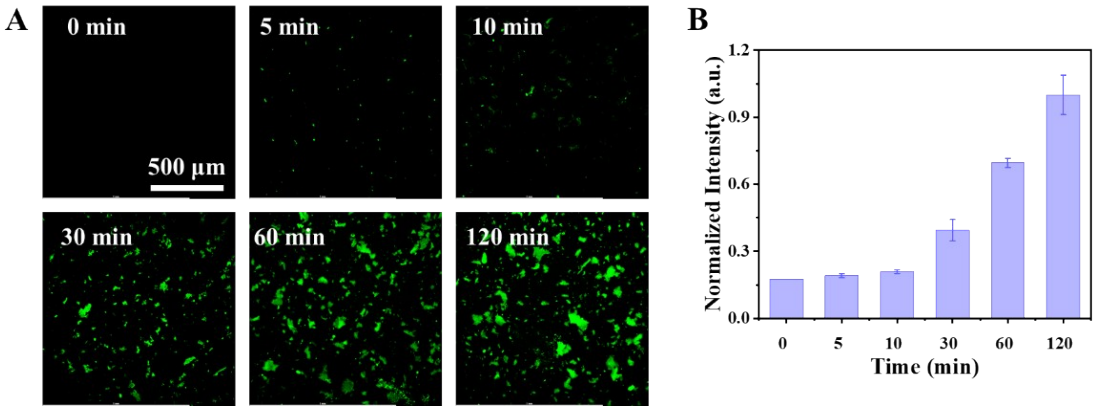

Figure S7. Time-dependent analysis of CmD binding to collagen. Fluorescence images (A) and the corresponding fluorescence signals (B) of a microplate immobilized with CmD in the presence of the type III collagen at different time points. Collagen III, 10 µg/mL; CmD, 1 µM. mCherry: E_x 555 nm/ E_m 610 nm. Scale bar, 500 µm.

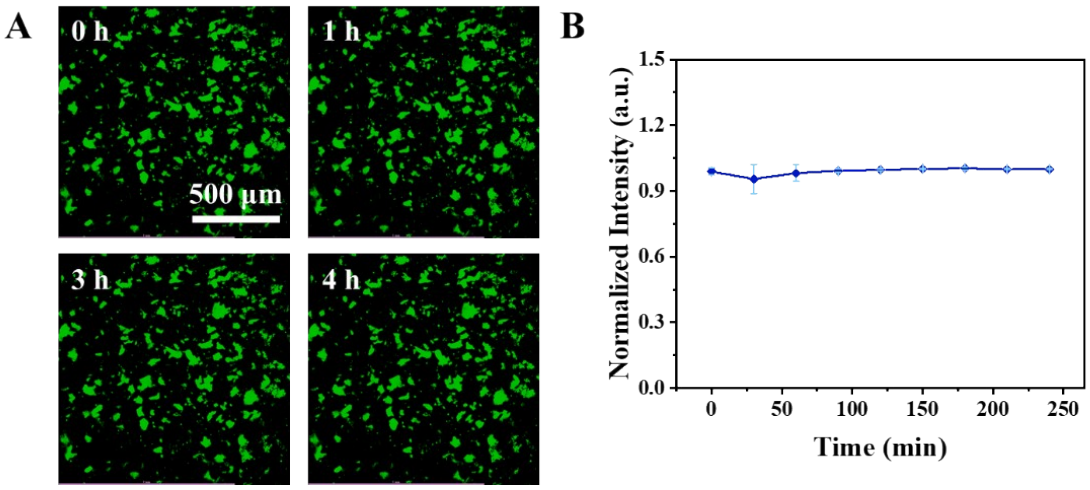

Figure S8. Stability analysis of CmD binding to collagen. Fluorescence images (left) and the corresponding fluorescence signals (right) of a microplate immobilized with CmD in the presence of the type III collagen over a 0-4 h duration. Collagen III, 10 μg/mL; CmD, 1 μM. mCherry: E_x 555 nm/ E_m 610 nm. Scale bar, 500 μm.

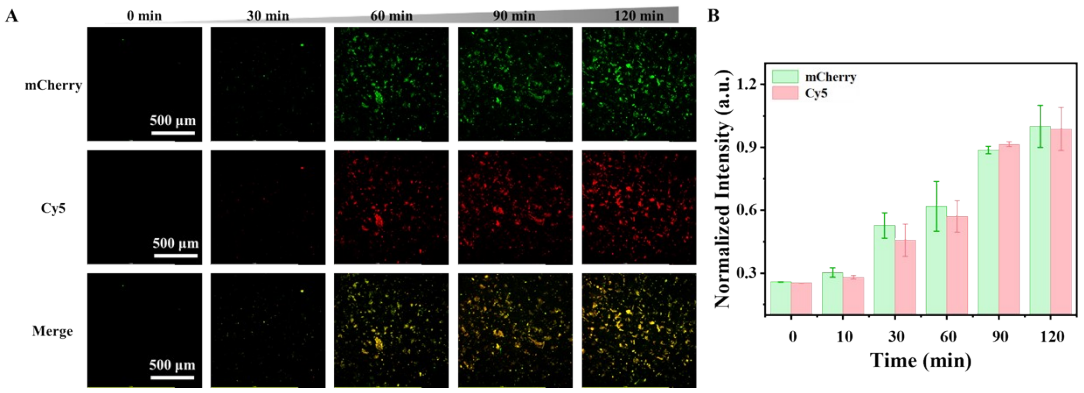

Figure S9. Fluorescence images (A) and quantitative analysis of the fluorescence intensities (B) of the collagen-coated wells pretreated with CmD-ssDNA$_{DCV}$-Cy5 at different time points. Collagen III, 10 μg/mL; CmD-ssDNA$_{DCV}$-Cy5, 1 μM. mCherry: E_x 555 nm/ E_m 610 nm; Cy5: E_x 635 nm/E_m 670 nm. Scale bar, 500 μm.

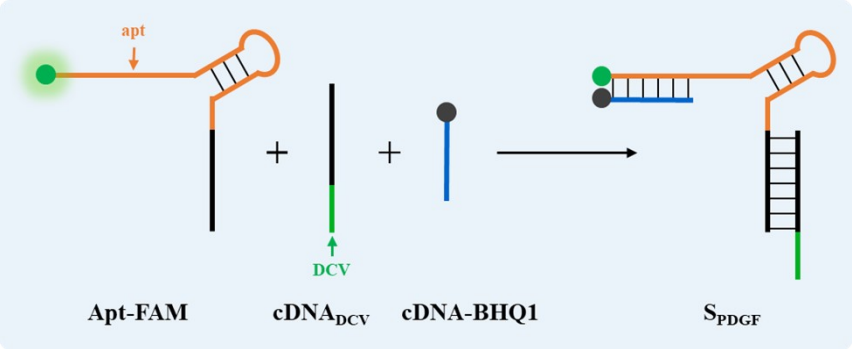

Figure S10. Schematic of the construction of S_{PDGF} used in this work.

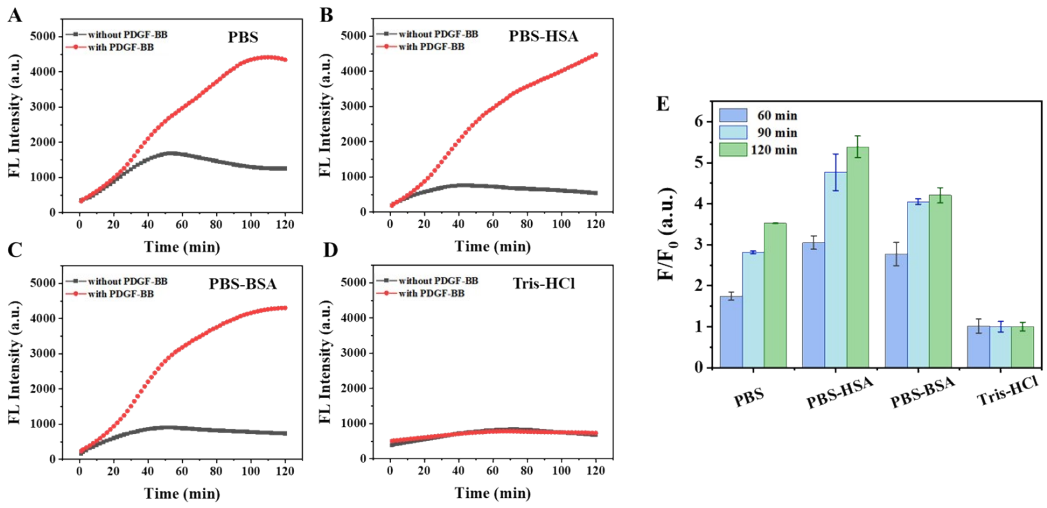

Figure S11. Evaluation of the effect of different buffer solutions on the analytical performance of S_{PDGF}. Fluorescence kinetic of S_{PDGF} response to PDGF-BB in PBS buffer (A), PBS-HSA buffer (B), PBS-BSA buffer (C), and Tris-HCl buffer (D), respectively. (E) Histograms display the corresponding value of F/F_0 of different buffers at different periods. F and F_0 correspond to the presence and absence of 50 nM PDGF-BB, respectively. S_{PDGF}, 20 nM. Data represent means ± SD.

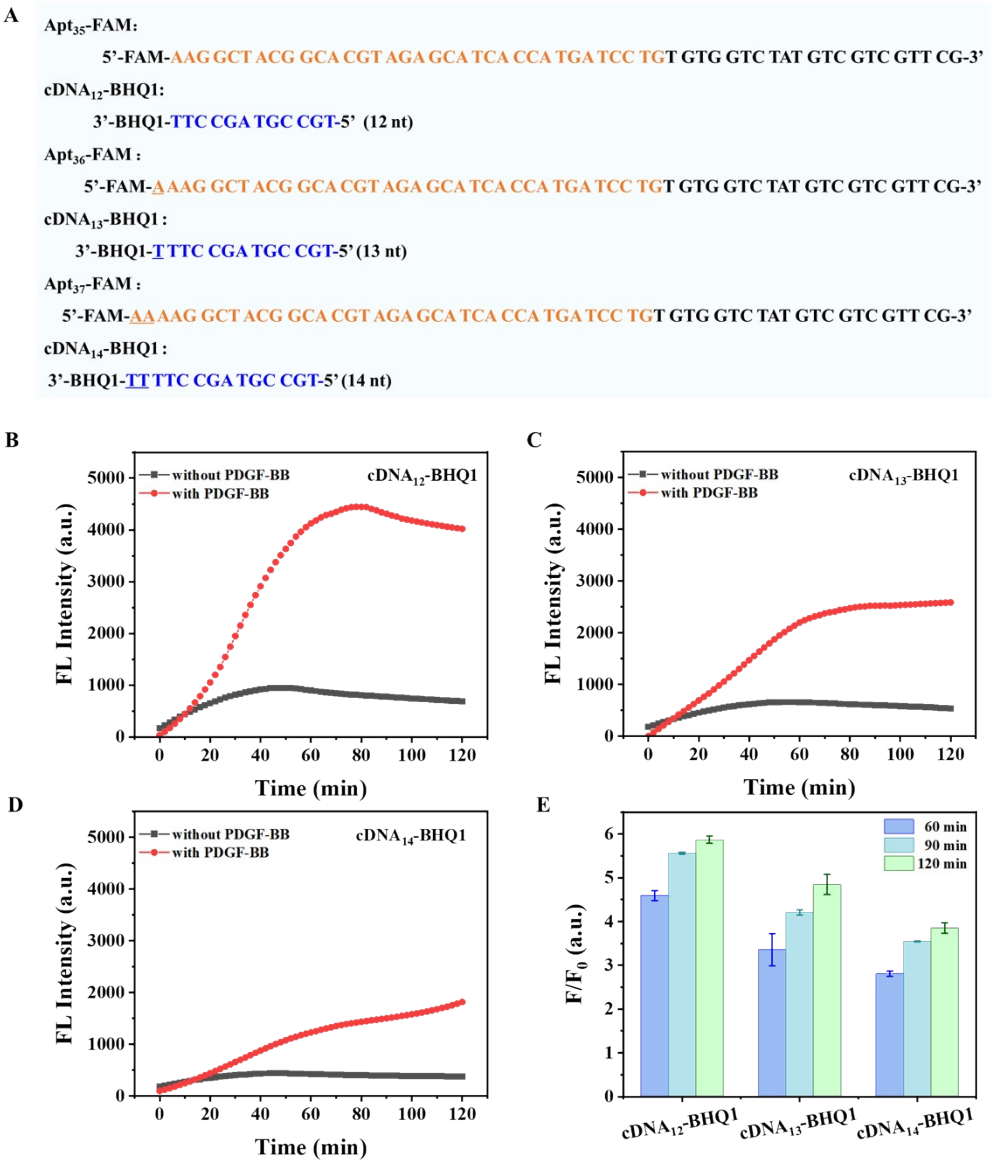

Figure S12. Effect of S_{PDGF} design on PDGF-BB detection. (A) Schematic representation of the S_{PDGF} design with three different hybridization lengths. The underlined bases indicate the extended length of the double-strand hybridization region in S_{PDGF}. Fluorescence kinetic analysis of PDGF-BB response in PBS-HSA buffer using S_{PDGF} probes designed with $cDNA_{12}$-BHQ1 (B), $cDNA_{13}$-BHQ1 (C), and $cDNA_{14}$-BHQ1 (D), respectively. (E) Histograms displaying the corresponding values of F/F_0 for the different S_{PDGF} probes at various periods. F and F_0 correspond to the presence and absence of 50 nM PDGF-BB, respectively. S_{PDGF}, 20 nM. Data represent means ± SD.

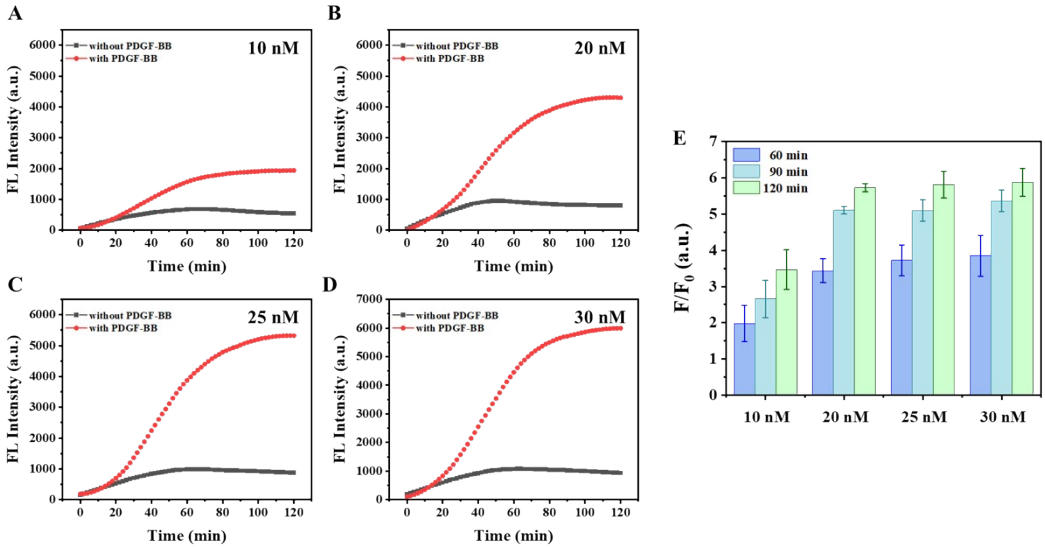

Figure S13. Effects of the concentration of S_{PDGF} probe on PDGF-BB detection. (A-D) Fluorescence kinetic analysis of PDGF-BB response in PBS-HSA buffer using S_{PDGF} at different concentrations (10 nM, 20 nM, 25 nM, and 30 nM). (E) Histograms displaying the corresponding values of F/F_0 for different concentrations of S_{PDGF} probe at various periods. F and F_0 correspond to the presence and absence of 50 nM PDGF-BB, respectively. Data represent means ± SD.

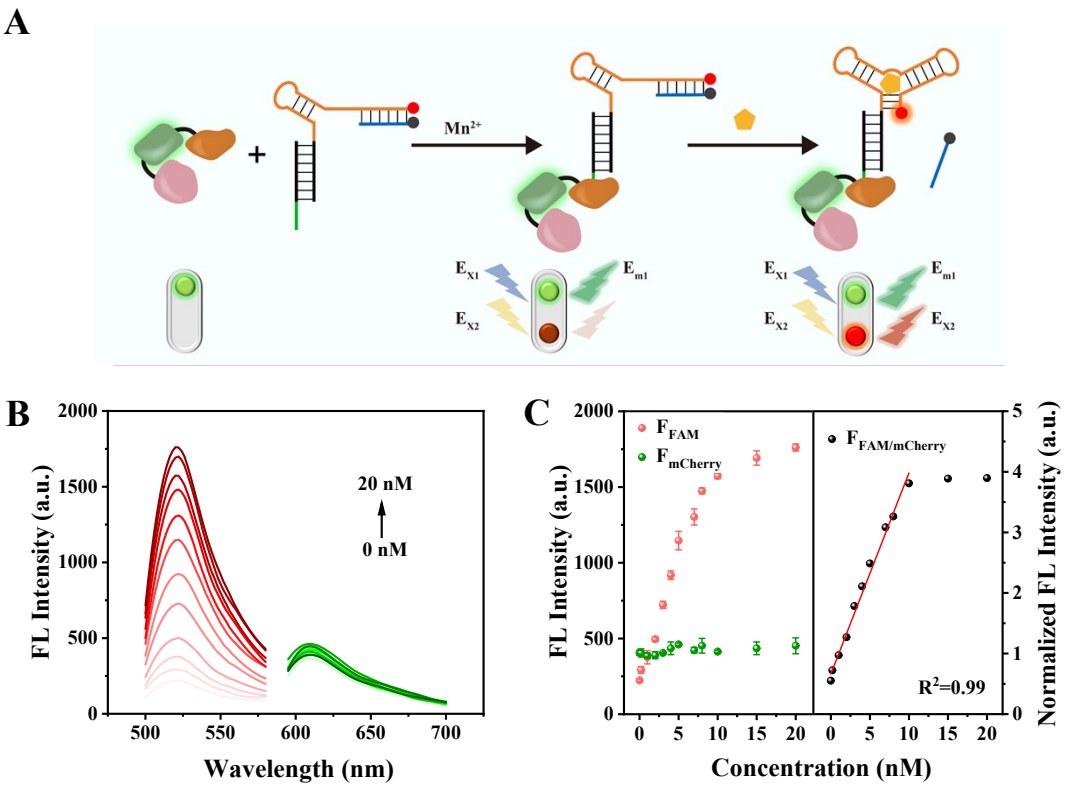

Figure S14. Design and sensitivity of the ratiometric probe **CPNN**$_{PDGF}$. (A) Schematic diagram of **CPNN**$_{PDGF}$ for PDGF-BB detection. (B) Fluorescence emission spectra of **CPNN**$_{PDGF}$ in response to different concentrations of PDGF-BB were obtained using the FAM channel (E_x 480 nm/E_m 520 nm) and mCherry channel (E_x 555 nm/E_m 610 nm). (C) Intensities of F_{FAM} and $F_{mCherry}$ (left) and $F_{FAM}/F_{mCherry}$ (right) signals as a function of PDGF-BB concentration. **CPNN**$_{PDGF}$, 20 nM. Data represent means ± SD.

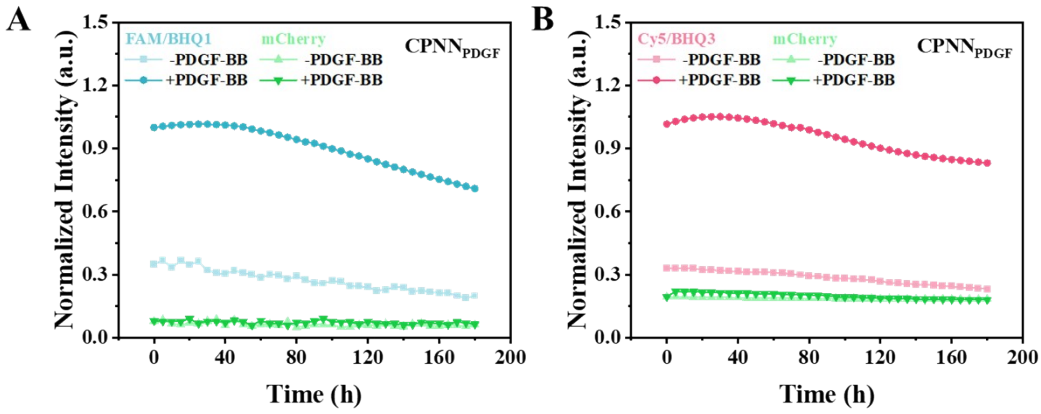

Figure S15. Photostability curves of **CPNN**$_{PDGF}$ labeled with FAM/BHQ1 (A) and Cy5/BHQ3 (B) after incubation with PDGF-BB. **CPNN**$_{PDGF}$, 20 nM; PDGF-BB, 20 nM.

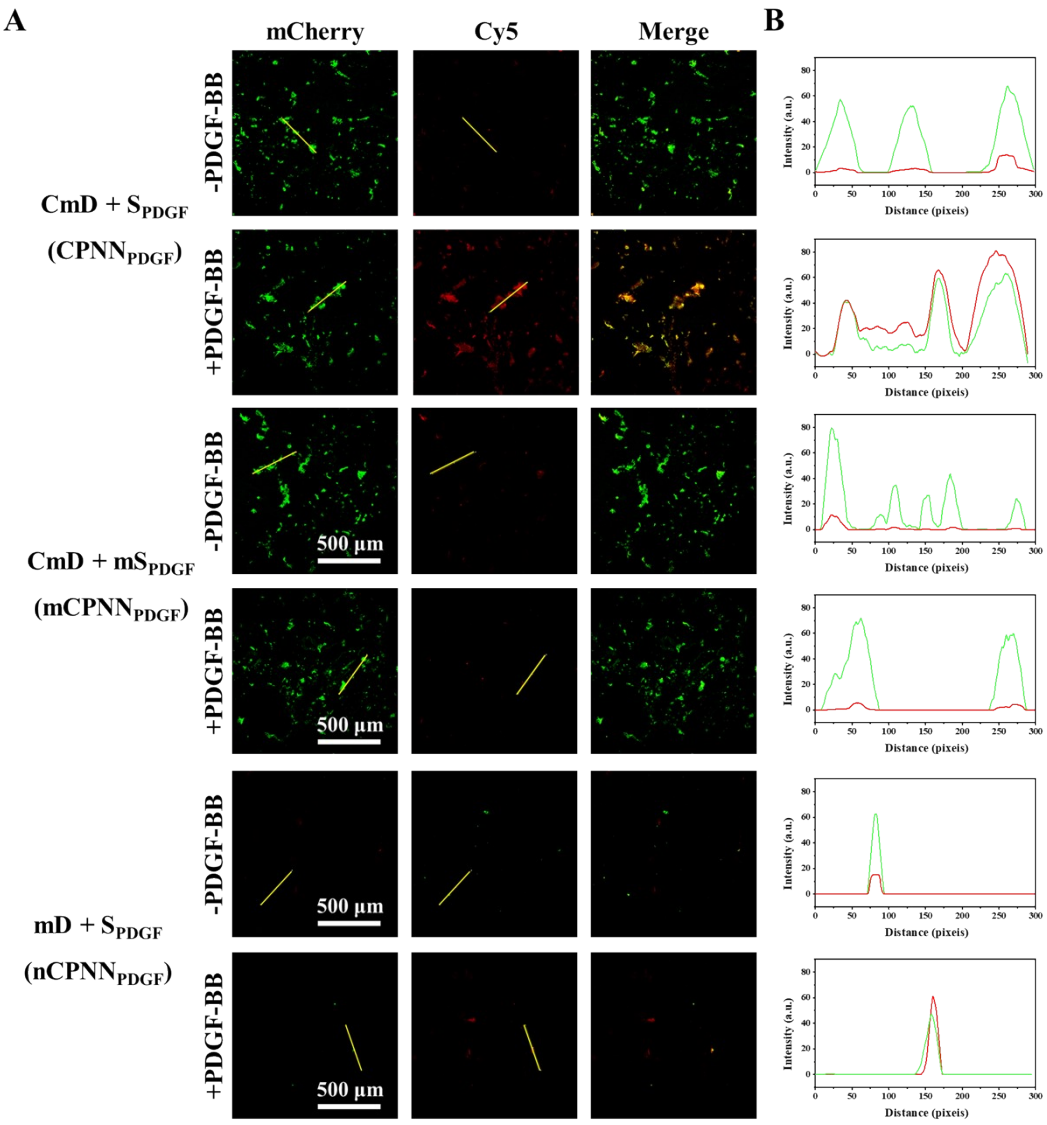

Figure S16. (A) Fluorescence imaging of the collagen III-coated wells treated with **CPNN**$_{PDGF}$ and control probes (**mCPNN**$_{PDGF}$ and **nCPNN**$_{PDGF}$). **mCPNN**$_{PDGF}$ was prepared by coupling CmD and mS$_{PDGF}$, while **nCPNN**$_{PDGF}$ was prepared by coupling mD and S$_{PDGF}$. (B) The intensity distribution of mCherry (green) and Cy5 (red) along the yellow arrows in panel (A). Collagen III, 10 μg/mL; **CPNN**$_{PDGF}$, 200 nM. mCherry: E_x 555 nm/ E_m 610 nm; Cy5: E_x 635 nm/E_m 670 nm. Scale bar, 500 μm.

A

Rabbit anti-Collagen I Antibody	+	-	+
Goat anti-Mouse IgG Secondary Antibody	+	-	-
Goat anti-Rabbit IgG Secondary Antibody	-	+	+

B

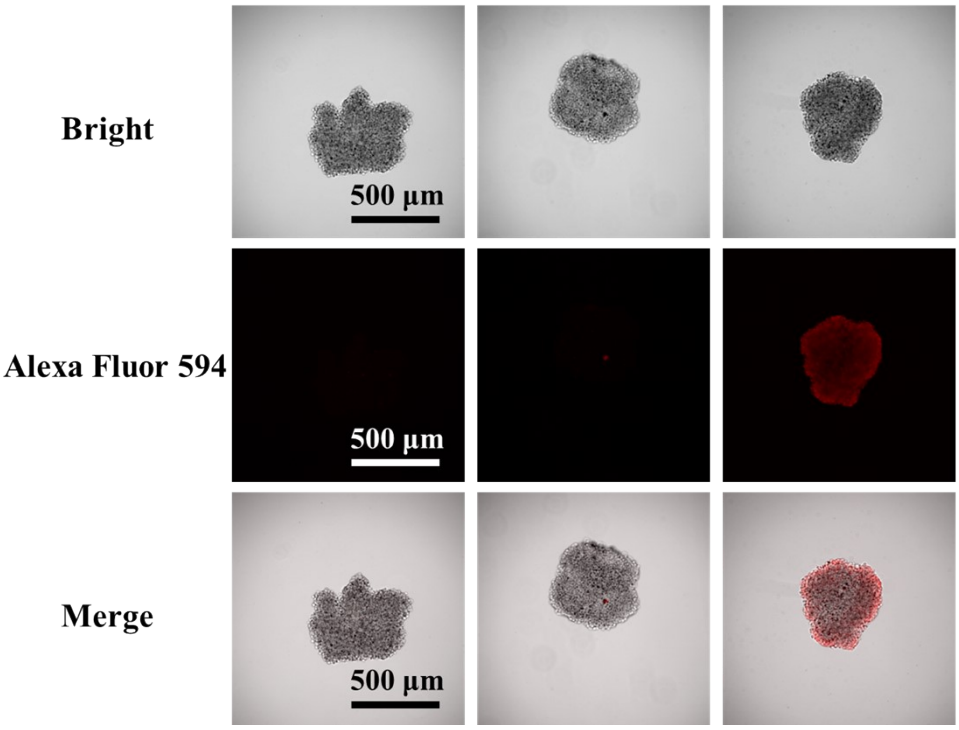

Figure S17. Immunofluorescence analysis of collagen in MCF-7 tumor spheroids. (A) Experimental design for immunofluorescence experiments conducted on the MCF-7 tumor spheroids. (B) Representative fluorescence image of collagen antibody immunofluorescence staining in fixed tumor spheroids. Alexa Fluor 594, E_x 575 nm/E_m 610 nm. Scale bar: 500 µm.

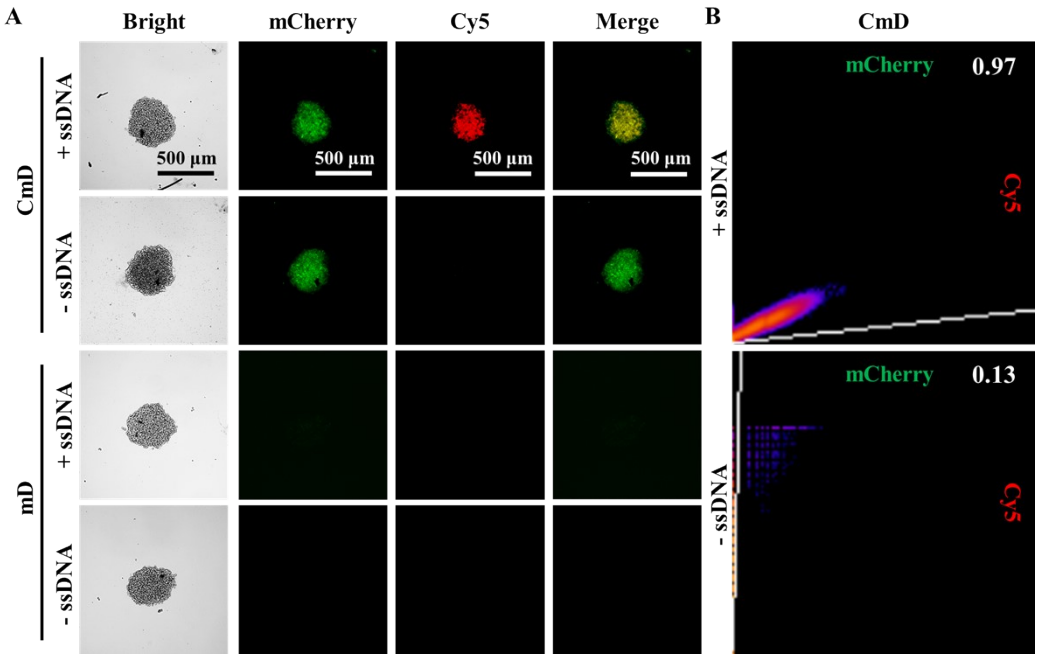

Figure S18. Investigating efficient targeting of CmD in MCF-7 tumor spheroids. (A) Fluorescence images of CmD or mD incubated with MCF-7 tumor spheroids in the presence or absence of $ssDNA_{DCV}$-Cy5. (B) Pearson configuration coefficients of mCherry and Cy5 for fluorescence images of MCF-7 tumor spheroids treated with CmD or CmD-$ssDNA_{DCV}$-Cy5. mCherry: E_x 555 nm/E_m 610 nm; Cy5: E_x 635 nm/E_m 670 nm. Scale bar, 500 μm.

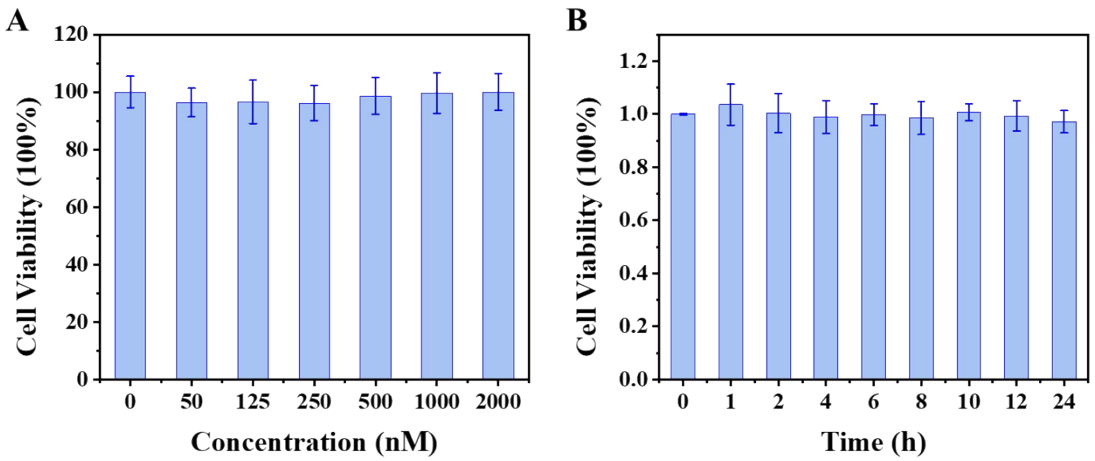

Figure S19. Cell viability of MCF-7 cells in the presence of CmD measured by CCK-8 assay. (A) Effect of the CmD concentration on the viability of MCF-7 cells. The cells were incubated with different concentrations of CmD for 24 h. (B) Impact of the incubation time on viability of MCF-7 cells after being incubated with 1 μM CmD for other times, respectively. All data represent means ± SD, n=5.

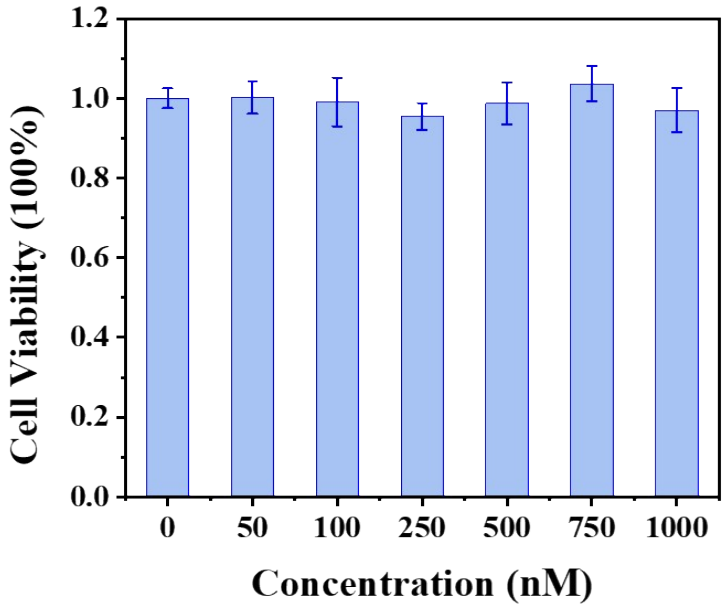

Figure S20. Effect of the **CPNN**$_{PDGF}$ concentration on the viability of MCF-7 cells. The cells were incubated with different concentrations of **CPNN**$_{PDGF}$ for 24 h. All data represent means ± SD, n=5.

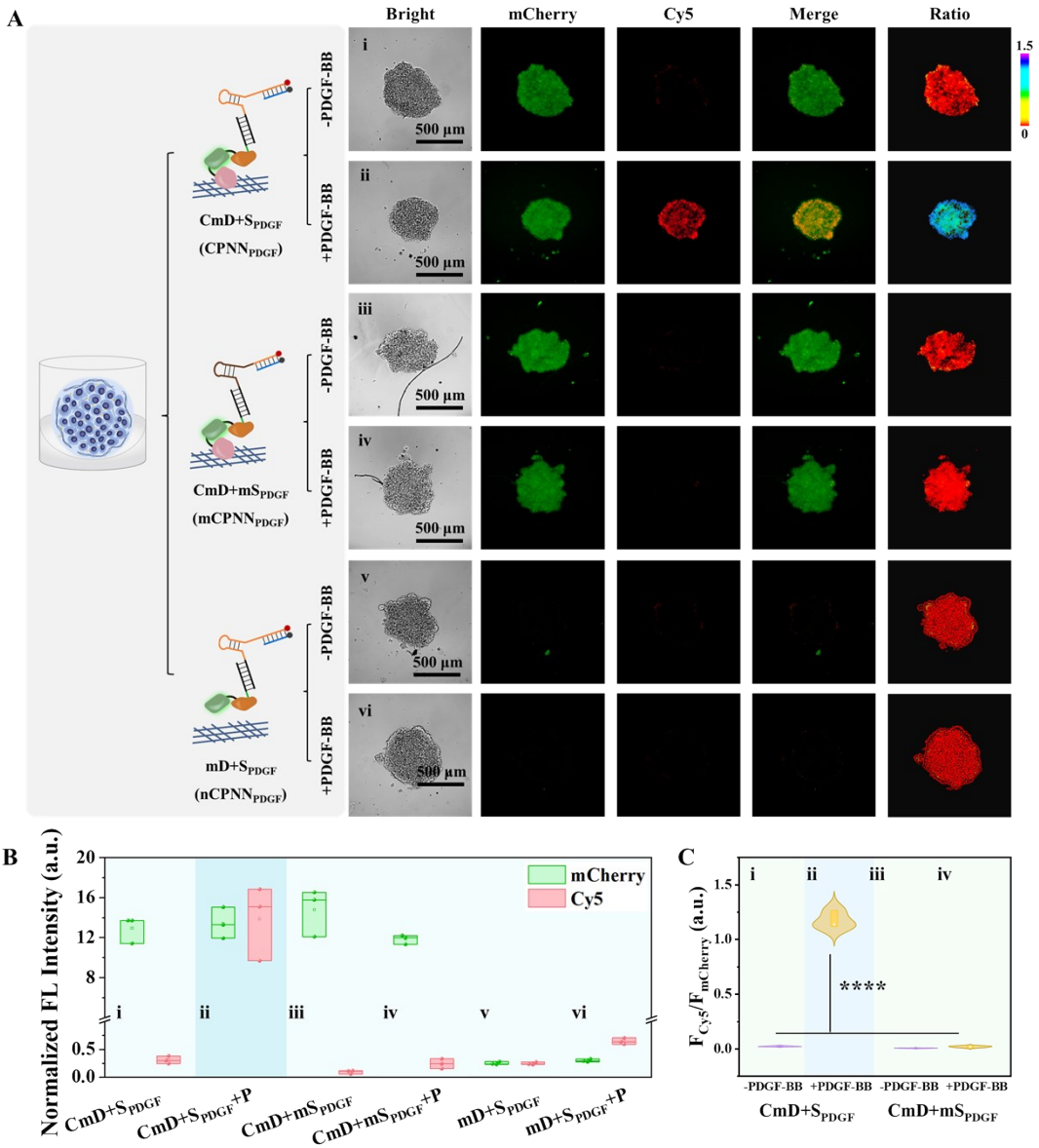

Figure S21. Evaluated the feasibility of **CPNN**$_{PDGF}$ for the sensing and imaging of PDGF-BB in MCF-7 tumor spheroids. (A) Fluorescence images of MCF-7 tumor spheroids pre-treated with **CPNN**$_{PDGF}$, **mCPNN**$_{PDGF}$, and **nCPNN**$_{PDGF}$, followed by incubation with or without PDGF-BB. Ratio images generated from the Cy5/mCherry channel. Relative fluorescence intensity of mCherry and Cy5 in differently treated MCF-7 tumor spheroids shown in panel A (B), along with the corresponding ratiometric signals $F_{Cy5}/F_{mCherry}$ (C). The treatment groups were as follows: (i) **CPNN**$_{PDGF}$, (ii) **CPNN**$_{PDGF}$ + PDGF-BB, (iii) **mCPNN**$_{PDGF}$, (iv) **mCPNN**$_{PDGF}$ + PDGF-BB, (v) **nCPNN**$_{PDGF}$, (vi) **nCPNN**$_{PDGF}$ + PDGF-BB. mCherry: E_x 555 nm/E_m 610 nm; Cy5: E_x 635 nm/E_m 670 nm. Scale bar, 500 μm.

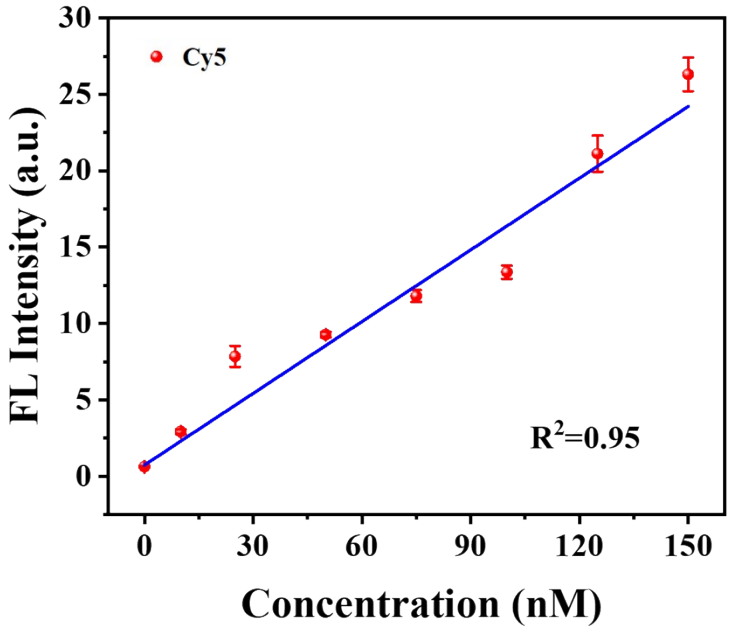

Figure S22. The intensities of Cy5 as a function of PDGF-BB concentration from imaging of the **CPNN**$_{PDGF}$ pretreated tumor spheroids.

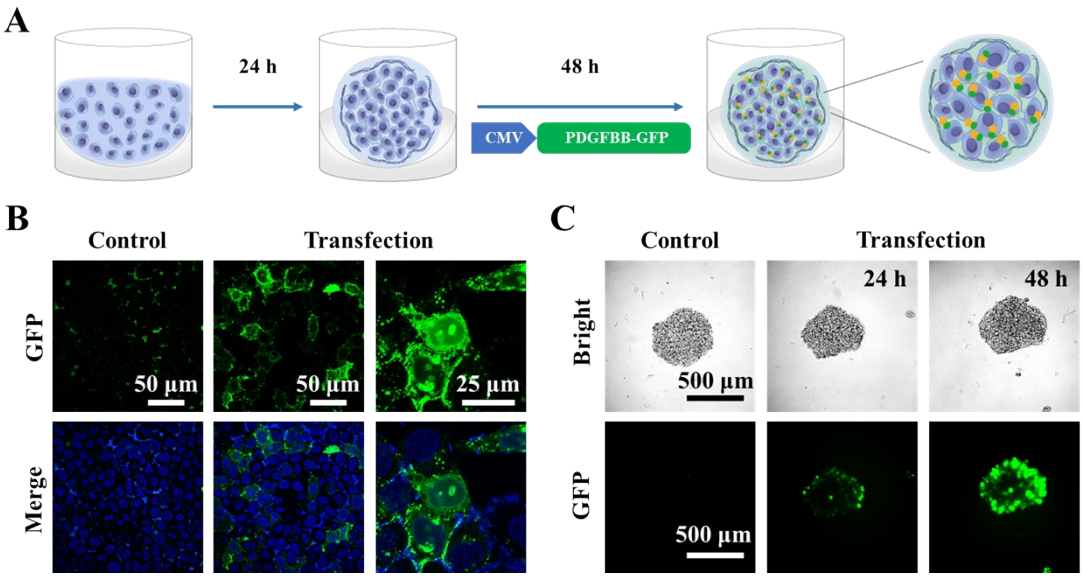

Figure S23. Schematic (A) and fluorescence imaging of PDGF-BB expression in the transfected MCF-7 cells (B) and tumor spheroids (C). Hoechst 33342: E_x 405 nm/E_m 460 nm; GFP: E_x 485 nm/E_m 520 nm. Scale bar, 500 μm.

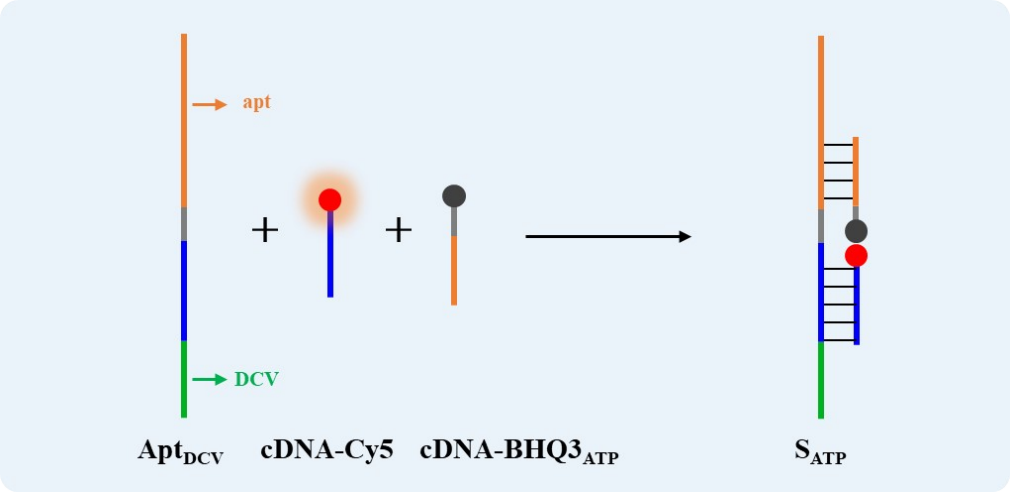

Figure S24. Schematic of the construction of the S_{ATP} used in this work.

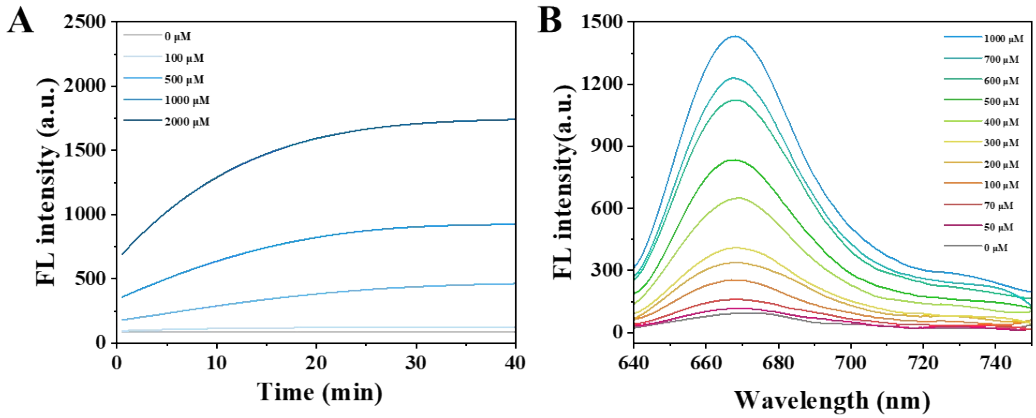

Figure S25. Evaluation of S_{ATP} for ATP detection in the buffer system. (A) Time-dependent fluorescence of S_{ATP} treated with different concentrations of ATP. (B) Fluorescence spectra of S_{ATP} responding to varying concentrations of ATP. S_{ATP} 200 nM. Data represent means ± SD.

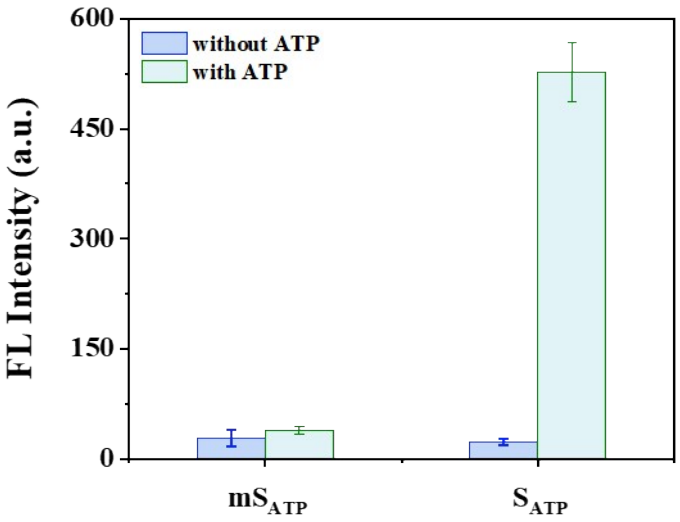

Figure S26. Fluorescence intensity of S_{ATP} and mS_{ATP} with and without the addition of ATP. S_{ATP} 200 nM; ATP, 1 mM. Data represent means ± SD.

Figure S27. Effect of the $\mathbf{CPNN}_{ATP}$ concentration on the viability of MCF-7 cells. The cells were incubated with different concentrations of $\mathbf{CPNN}_{ATP}$ for 24 h. All data represent means ± SD, n=5.

Reference

1 Hu SF, Zhang JH, Tang R, Fan JH, Liu HQ, Kang WY, Lei CY, Nie Z, Huang Y. *Anal Chem*, 2019, 91(15): 10180-10187

2 Deng HH, Liu HQ, Kang WY, Lei CY, Nie Z, Huang Y, Yao SZ. *Nanoscale*, 2020, 12(2): 864-870

3 Mansurov A, Ishihara J, Hosseinchi P, Potin L, Marchell TM, Ishihara A, Williford JM, Alpar AT, Raczy MM, Gray LT, Swartz MA, Hubbell JA. *Nat Bio med Eng*, 2020, 4(5): 531-543

4 Zhang JH, Li HY, Lin B, Luo XY, Yin P, Yi T, Xue BB, Zhang XL, Zhu HZ and Nie Z, *J Am Chem Soc*, 2021, 143, 19317-19329

5 Wang S, Zhang ZH, Wei SH, He F, Li Z, Wang HH, Huang Y, Nie Z. *Acta Biomater*, 2021, 130: 138-148

6 A. Povedailo V, L. Lysenko I, A. Tikhomirov S, L. Yakovlev D, A. Tsybulsky D, S. Kruhlik A, F. Fan, V. Martynenko-Makaev Y, L. Sharko O, V. Duong P, H. Minh P and V. Shmanai V, *J Fluoresc*, 2020, 30, 629-635

7. Mukherjee S, Manna P, Hung ST, Vietmeyer F, Friis P, E. Palmer A and Jimenez R, *J Phys Chem B*, 2022, 126, 4659-4668

8. Schobel U, Egelhaaf HJ, Brecht A, Oelkrug D and Gauglitz G, Bioconjugate Chem, 1999, 10, 1107-1114